Measurements of the Dark Matter Mass, Temperature and Spin

Bruce Hoeneisen

Universidad San Francisco de Quito, Quito, Ecuador
Email: bhoeneisen@usfq.edu.ec
11 August 2024

Abstract

We summarize several measurements of the dark matter temperature-to-mass ratio, or equivalently, of the comoving root-mean-square thermal velocity of warm dark matter particles $v_{h\mathrm{rms}}(1)$. The most reliable determination of this parameter comes from well measured rotation curves of dwarf galaxies by the LITTLE THINGS collaboration: $v_{h\mathrm{rms}}(1) = 406 \pm 69$ m/s. Complementary and consistent measurements are obtained from rotation curves of spiral galaxies measured by the SPARC collaboration, density runs of giant elliptical galaxies, galaxy ultra-violet luminosity distributions, galaxy stellar mass distributions, first galaxies, and reionization. Having measured $v_{h\mathrm{rms}}(1)$, we then embark on a journey to the past that leads to a consistent set of measured dark matter properties, including mass, temperature and spin.

Keywords Warm Dark Matter, Dwarf Galaxies, Spiral Galaxies, Elliptical Galaxies, Galaxy Distributions, First Galaxies, Reionization.

1 Introduction

Most of the non-relativistic matter in the universe, 84.3 ± 0.2 % [1], is in a "dark matter" form that has only been "observed" through its gravitational interaction. If this dark matter is a gas of particles of mass m_h, this mass is unknown in the range 10^{-22} eV to $10^{+67}\mathrm{eV} = 5\mathrm{M}_\odot$ [1], i.e. over 89 orders of magnitude! Let us consider non-relativistic dark matter at a time when the universe is nearly homogeneous. Let $\rho_h(a)$ be the density of dark matter, and $v_{h\mathrm{rms}}(a)$ be the root-mean-square thermal velocity of the dark matter

Table 1: Summary of measurements of the warm dark matter particle comoving root-mean-square thermal velocity $v_{h\mathrm{rms}}(1)$.

Observable	$v_{h\mathrm{rms}}(1)$	Fig. or Sec.	Reference
Dwarf galaxies	406 ± 69 m/s	Fig. 2	[4]
Spiral galaxies	≈ 450 m/s *	Fig. 4	[5]
Elliptical galaxies	≈ 450 m/s *	Fig. 6	[6]
Stellar mass distrib.	250 to 750 m/s	Fig. 7	[7]
UV luminosity distrib.	281 ± 94 m/s	Fig. 7	[7]
First galaxies	360 ± 110 m/s	Section 5	[8]
Reionization	150 to 1200 m/s	Section 6	[8]

* Lower bound of distribution.

particles. $a(t)$ is the expansion parameter of the universe, normalized to $a(t_0) = 1$ at the present time t_0. Due to the expansion of the universe, $v_{h\mathrm{rms}}(a)$ varies in proportion to a^{-1} [2], and $\rho_h(a)$ varies in proportion to a^{-3}, so

$$v_{h\mathrm{rms}}(1) \equiv v_{h\mathrm{rms}}(a)a = v_{h\mathrm{rms}}(a) \left(\frac{\Omega_c \rho_{\mathrm{crit}}}{\rho_h(a)} \right)^{1/3} \tag{1}$$

is an adiabatic invariant. $\Omega_c \rho_{\mathrm{crit}}$ is the present dark matter density of the universe (throughout we use the standard notation and parameter values of [1]). In the present article we summarize measurements of the parameter $v_{h\mathrm{rms}}(1)$, and let the data decide whether dark matter is cold or warm. The results are collected in Table 1, and will be explained in the following Sections. Full details of each measurement can be found in the references listed in Table 1.

We are then in a position to extrapolate these results to the past. Note that dark matter becomes ultra-relativistic at expansion parameter $a_{h\mathrm{NR}} \approx v_{h\mathrm{rms}}(1)/c$. It turns out that if we assume the ultra-relativistic dark matter has zero chemical potential [2], then we obtain a self-consistent set of measurements of the dark matter mass, temperature and spin [3].

2 Measurements of $v'_{h\mathbf{rms}}(1)$ in Galaxy Cores

Consider a free observer in a density peak in the early universe. Due to the expansion of the universe, this observer sees dark matter expand adiabatically, i.e. conserving $v_{h\mathrm{rms}}(1) \equiv v_{h\mathrm{rms}}(a)a$ [2], reach maximum expansion, and then contract into the core of a galaxy. Good fits to the data are obtained assuming that, in the radial range r from $r_{\min}$ to $r_{\max}$, the galaxy is a

self-gravitating gas of "baryons" and dark matter, each separately in thermal equilibrium [2]. "Baryons" are stars (live and dead), neutral and ionized gas, and dust. These two components have similar root-mean-square velocities, and therefore have different temperatures, so the interaction of dark matter particles with baryons can be neglected on galactic scales. The following observable can be measured in the core of galaxies (away from the central black hole if any):

$$v'_{h\mathrm{rms}}(1) \equiv \sqrt{3\left\langle v_{rh}^2 \right\rangle}\left(\frac{\Omega_c \rho_{\mathrm{crit}}}{\rho_h(r_{\mathrm{min}})}\right)^{1/3}, \tag{2}$$

where the radial root-mean-square thermal velocity $\sqrt{\left\langle v_{rh}^2 \right\rangle}$ is independent of r in the range from r_{min} to r_{max}. If the contraction of dark matter into the core of the galaxy were adiabatic we would have

$$v'_{h\mathrm{rms}}(1) = v_{h\mathrm{rms}}(1). \tag{3}$$

However, due to relaxation [6] and rotation [5], we expect

$$v'_{h\mathrm{rms}}(1) \gtrsim v_{h\mathrm{rms}}(1). \tag{4}$$

If dark matter is warm, first galaxies have a threshold mass due to velocity dispersion [9] [10]. For these first dwarf galaxies we expect $v'_{h\mathrm{rms}}(1)$ to be nearly equal to $v_{h\mathrm{rms}}(1)$. We expect $v'_{h\mathrm{rms}}(1)$ to increase for massive spiral and elliptical galaxies, mainly due to relaxation in the merger of galaxies during the hierarchical formation of structure [6]. By comparing the distributions of $v'_{h\mathrm{rms}}(1)$ in dwarf and in massive spiral and elliptical galaxies, we can estimate the importance of relaxation and dark matter halo rotation.

The galaxy, considered as a self-gravitating gas of baryons and dark matter, separately in thermal equilibrium in the radial range r from r_{min} to r_{max}, is described by the following hydrostatic equations [2]:

$$\nabla \cdot \mathbf{g}_b = -4\pi G\rho_b, \qquad \nabla \cdot \mathbf{g}_h = -4\pi G\rho_h, \tag{5}$$

$$\mathbf{g} = \mathbf{g}_b + \mathbf{g}_h - \frac{GM_{\mathrm{BH}}}{r^2}\hat{\mathbf{e}}_r = -\frac{V(r)^2}{r}\hat{\mathbf{e}}_r, \tag{6}$$

$$\nabla P_b = \rho_b\left(\mathbf{g} + \kappa_b\frac{V(r)^2}{r}\hat{\mathbf{e}}_r\right), \tag{7}$$

$$\nabla P_h = \rho_h\left(\mathbf{g} + \kappa_h\frac{V(r)^2}{r}\hat{\mathbf{e}}_r\right), \tag{8}$$

$$P_b = \left\langle v_{rb}^2 \right\rangle \rho_b, \qquad \text{and} \qquad P_h = \left\langle v_{rh}^2 \right\rangle \rho_h. \tag{9}$$

Sub-indices b and h stand for baryons and for the dark matter halos, respectively. Equations (5) and (6) are Newton's equations. $V(r)$ is the rotation

velocity of a test particle. Equations (7) and (8) express conservation of momentum [2]. Equations (9) are equations of state of classical, i.e. non-degenerate, gases (justified by the excellent fits to the data, and by arguments in Section 7 below). We note that $\langle v_{rb}^2 \rangle$ and $\langle v_{rh}^2 \rangle$ are independent of r from $r_{\rm min}$ to $r_{\rm max}$. The parameters κ_b and κ_h describe baryon and dark matter rotation (nominally $\kappa_b \approx 0.98$ and $\kappa_h \approx 0.15$ in spiral galaxies [11]). These hydrostatic equations are justified because they obtain excellent fits to the data, and are valid whether or not dark matter is collisional [2].

We integrate numerically the hydrostatic equations from $r_{\rm min}$ to $r_{\rm max}$. To this end we need to specify the following boundary conditions: $\sqrt{\langle v_{rb}^2 \rangle /(1-\kappa_b)}$, $\sqrt{\langle v_{rh}^2 \rangle /(1-\kappa_h)}$, $\rho_b(r_{\rm min})$, $\rho_h(r_{\rm min})$, and the central black hole mass $M_{\rm BH}$. (To obtain directly the uncertainty of $v'_{h\rm rms}(1)$ we can replace $\rho_h(r_{\rm min})$ by $v'_{h\rm rms}(1)$ of (2) in the fit.) These boundary conditions are varied to minimize a χ^2 between the calculations and the measured galaxy rotation curves or density runs. In this way we are able to measure $v'_{h\rm rms}(1)$ for each galaxy (see the references in Table 1 for full details of the fits to each galaxy).

In Fig. 1 we present the fit to the rotation curves of 36 co-added dwarf galaxies. This fit obtains $v'_{h\rm rms}(1) = 515 \pm 15$ (stat) m/s. We seek the lower bound of the distribution of $v'_{h\rm rms}(1)$, that we identify with $v_{h\rm rms}(1)$. The distribution of $v'_{h\rm rms}(1)$ of 11 well measured dwarf galaxies by the *Local Irregulars That Trace Luminosity Extremes, The Hi Nearby Galaxy Survey* (LITTLE THINGS) collaboration [12] is presented in Fig. 2. This distribution has a narrow peak at

$$v_{h\rm rms}(1) = 406 \pm 69 \text{ m/s}. \tag{10}$$

Since relaxation and dark matter halo rotation can only increase the observed $v'_{h\rm rms}(1)$, we interpret the few galaxies to the right of this peak to have non-negligible relaxation.

A fit to the rotation curves of a massive spiral galaxy is shown in Fig. 3. This fit obtains $v'_{h\rm rms}(1) = 535 \pm 8$ (stat) m/s. The distribution of $v'_{h\rm rms}(1)$ of 40 spiral galaxy rotation curves, measured by the *Spitzer Photometry and Accurate Rotation Curves* (SPARC) collaboration [14], is presented in Fig. 4. The lower bound of this distribution has $v_{h\rm rms}(1) \approx 450$ m/s, in agreement with the peak in the distribution of first generation dwarf galaxies in Fig. 2. The width of the distribution in Fig. 4 is interpreted to be due to relaxation (and dark matter halo rotation) acquired mainly during galaxy mergers during the hierarchical formation of structure. Note that the correction for relaxation is at most a factor 3 in massive galaxies.

The fit to the measured density runs of the giant elliptical galaxy J1313+4615 is presented in Fig. 5. This fit obtains $v'_{h\rm rms}(1) = 784 \pm 304$ (stat) m/s. The distribution of $v'_{h\rm rms}(1)$ of 23 giant elliptical galaxies is presented in Fig. 6.

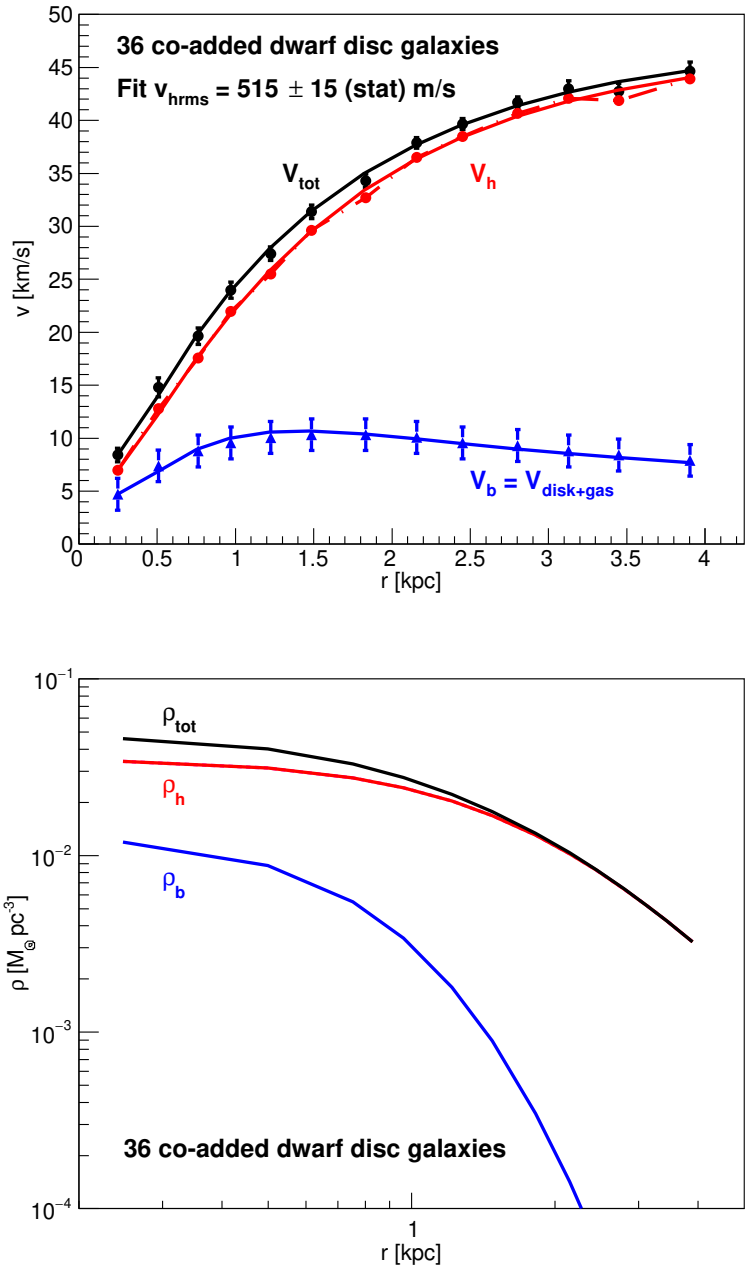

Figure 1: Rotation curves and densities of dwarf disk galaxies. The data is the average of the rotation curves of 36 dwarf disk galaxies re-scaled to their average optical radius $R_{\rm opt} = 2.5$ kpc and corresponding rotation velocity $V_{\rm opt} = 40$ km/s (from Fig. 7 of [13]). The curves are the solution of the hydrostatic equations as explained in the text. Figure from [6].

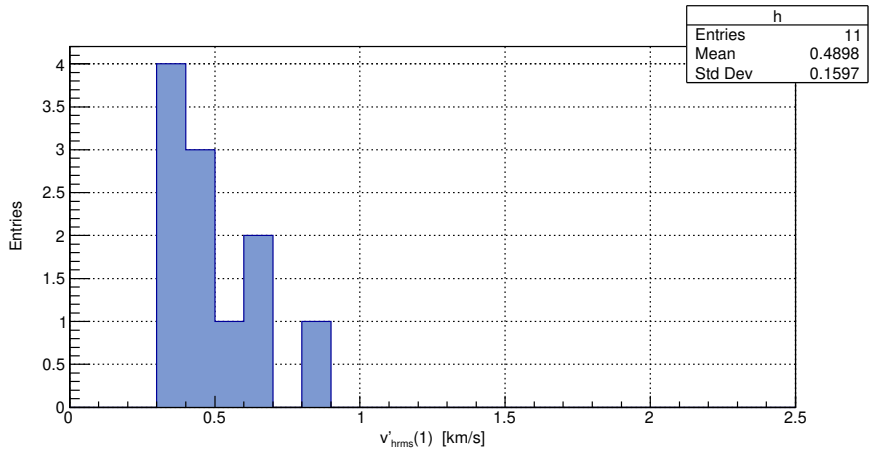

Figure 2: Distribution of $v'_{h\mathrm{rms}}(1)$, i.e. the adiabatic invariant before the dark matter rotation and relaxation correction, of 11 dwarf galaxies measured by the LITTLE THINGS collaboration [12]. These corrections can only be negative, and so are negligible in the peak at $v'_{h\mathrm{rms}}(1) \approx v_{h\mathrm{rms}}(1) \approx 406 \pm 69$ m/s. Figure from [4].

The data is from Fig. 12 of [15]. The total densities $\rho_{\mathrm{tot}}(r)$ are measured with strong lensing, weak lensing and kinematic constraints, while the baryon densities $\rho_b(r)$ are obtained from Hubble Space Telescope imaging data with several filters. The width of the distribution in Fig. 6 is due to the large statistical uncertainties of these measurements of $v'_{h\mathrm{rms}}(1)$ (because the cores are dominated by baryons), and to the relaxation of galaxy mergers in the hierarchical formation of structure. Again, the lower bound of the distribution is consistent with the lower bounds of the distributions for spiral and dwarf galaxies.

We note that the absolute luminosities of these galaxies span 4 orders of magnitude, and the baryon core densities span 6 orders of magnitude [6], so we interpret the lower bound of these distributions to be of cosmological origin, i.e $v_{h\mathrm{rms}}(1)$. This interpretation is reinforced by independent measurements of $v_{h\mathrm{rms}}(1)$ presented in the following Sections.

3 Free-Streaming

Let $P(k)$ be the comoving power spectrum of density perturbations in the standard lambda cold dark matter (ΛCDM) cosmological model. If dark

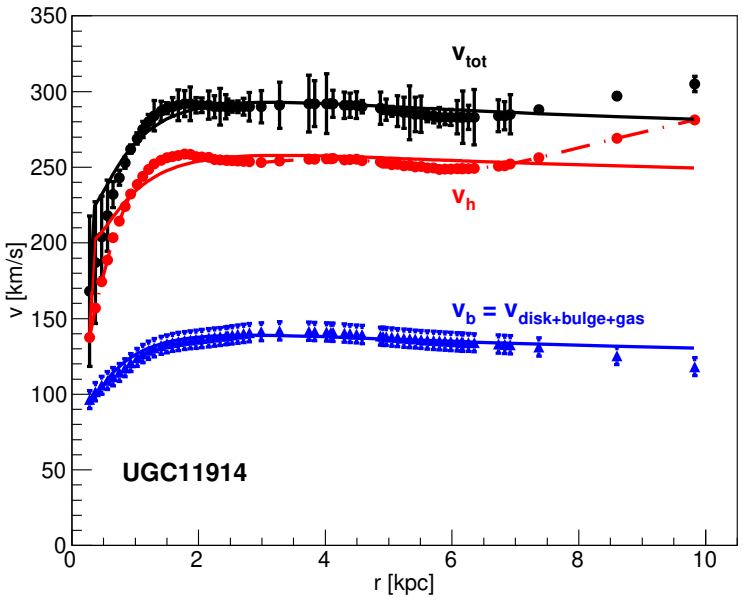

Figure 3: Observed rotation curve $V_{\rm tot}(r)$ (dots) and the baryon contribution $V_b(r)$ (triangles) of the giant spiral galaxy UGC11914 measured by the SPARC collaboration [14]. The solid lines are obtained by numerical integration as explained in the text. Figure from [2].

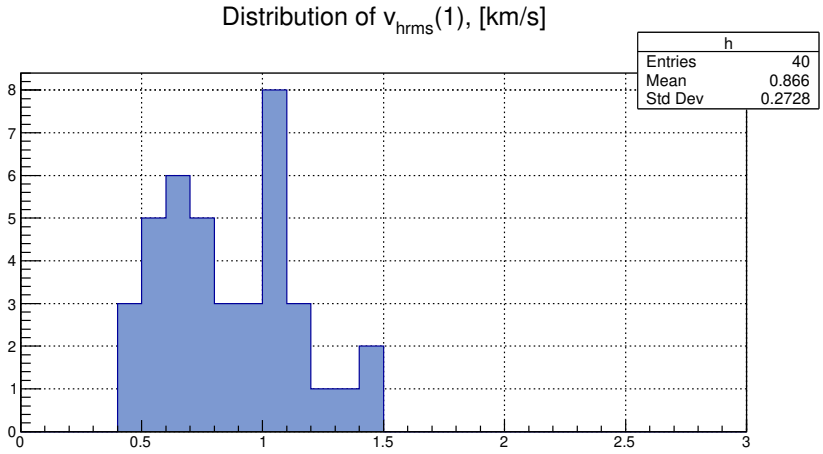

Figure 4: Distribution of $v'_{h\mathrm{rms}}(1)$ obtained from fits to the rotation curves of 40 spiral galaxies measured by the SPARC collaboration [14]. Figure from [5].

matter is warm instead of cold, then the power spectrum at large comoving wavevector k becomes suppressed by a cut-off factor $\tau^2(k)$ due to warm dark matter free-streaming in and out of density minimums and maximums: $P_{\mathrm{WDM}}(k) \equiv P(k)\tau^2(k)$.

The cut-off factor, obtained by solving exactly the linearized collisionless Boltzmann-Vlasov equation [16], can be approximated, at the time t_{eq} of equal radiation and matter densities, as

$$\tau^2(k) \approx \exp\left[-k^2/k^2_{\mathrm{fs}}(t_{\mathrm{eq}})\right], \qquad \text{with} \tag{11}$$

$$k_{\mathrm{fs}}(t_{\mathrm{eq}}) = \frac{1.455}{\sqrt{2}}\sqrt{\frac{4\pi G\Omega_c\rho_{\mathrm{crit}}a_{\mathrm{eq}}}{v_{h\mathrm{rms}}(1)^2}}. \tag{12}$$

At later times the Jeans mass decreases as $a^{-3/2}$, so non-linear regeneration of small scale structure becomes possible, and gives $\tau^2(k)$ a "tail" when relative density perturbations approach unity. At the times of galaxy formation, we take

$$\begin{aligned}\tau^2(k) &= \exp\left(-\frac{k^2}{k^2_{\mathrm{fs}}(t_{\mathrm{eq}})}\right) \qquad \text{if } k < k_{\mathrm{fs}}(t_{\mathrm{eq}}),\\ &= \exp\left(-\frac{k^n}{k^n_{\mathrm{fs}}(t_{\mathrm{eq}})}\right) \qquad \text{if } k \geq k_{\mathrm{fs}}(t_{\mathrm{eq}}),\end{aligned} \tag{13}$$

where n is *measured* to be in the range $0.5 \lesssim n \lesssim 1.1$ [8].

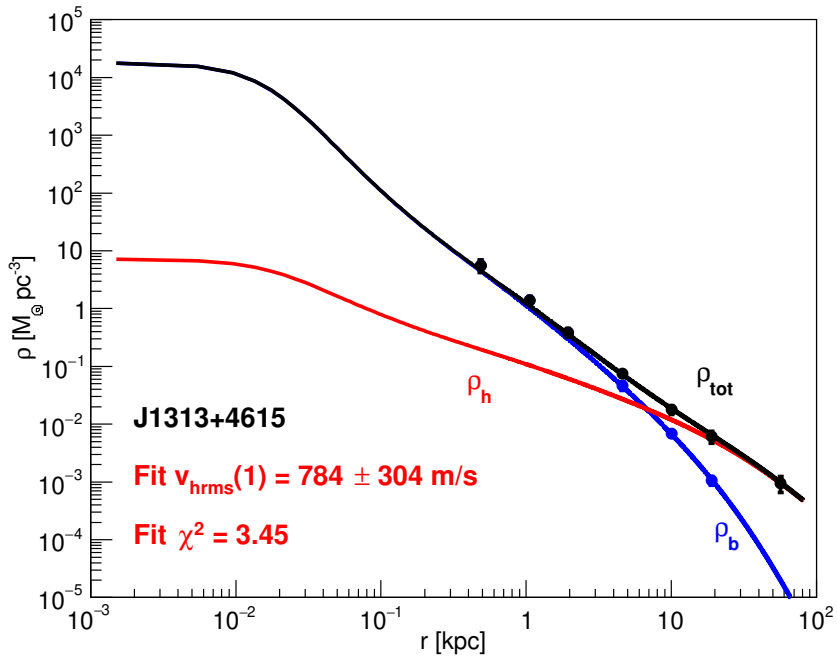

Figure 5: Observed [15] and calculated densities $\rho_{\rm tot}(r)$, $\rho_b(r)$ and $\rho_h(r)$ of the giant elliptical galaxy J1313+4615. The fitted parameters are $\sqrt{\langle v_{rb}^2\rangle}$, $\sqrt{\langle v_{rh}^2\rangle}$, $\rho_b(r_{\rm min})$ and $v'_{h\rm rms}(1)$. Freeing a central black hole mass $M_{\rm BH} = 0$ does not change the fit significantly. Note that the dark matter core is too small to be resolved in most observations or simulations. Figure from [6].

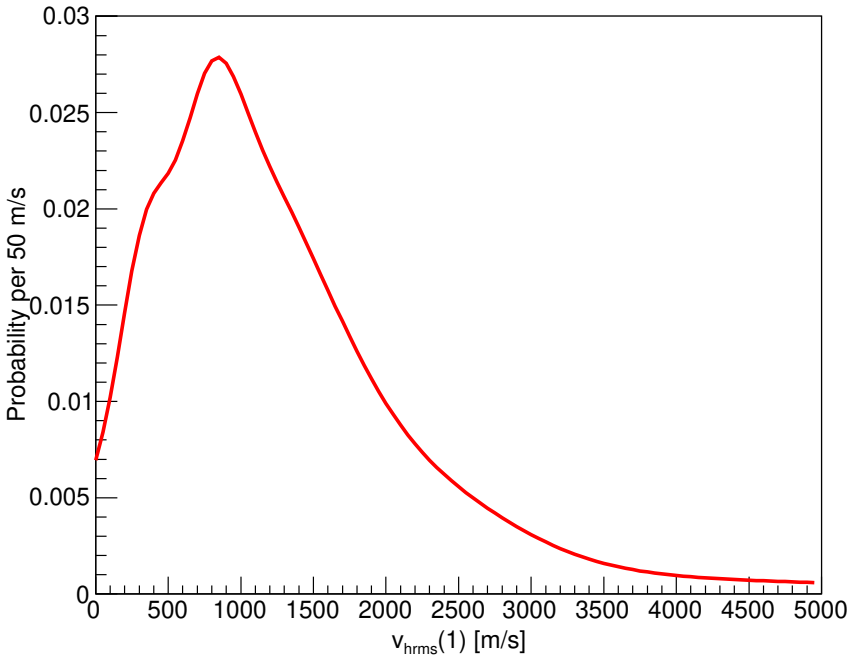

Figure 6: Distribution of the measured $v'_{h\mathrm{rms}}(1)$ of 23 massive elliptical galaxies. The data is from Fig. 12 of [15]. Figure from [6].

4 Measurements of $k_{\rm fs}$ with Galaxy Distributions

From galaxy stellar mass distributions for redshifts $z = 4, 5, 6, 7$ and 8 [7], we estimate 3 Mpc$^{-1} \gtrsim k_{\rm fs} \gtrsim 1$ Mpc^{-1}, corresponding to 250 m/s $\lesssim v_{h\rm rms}(1) \lesssim$ 750 m/s. See Fig. 7 for redshift $z = 6$.

From galaxy UV luminosity distributions for redshift z in the wide range 2, 3, 4... to 13 [7], we estimate 4 Mpc$^{-1} \gtrsim k_{\rm fs} \gtrsim 2$ Mpc^{-1}, corresponding to 187 m/s $\lesssim v_{h\rm rms}(1) \lesssim 375$ m/s. See Fig. 7 for redshift $z = 6$.

5 Estimates of $k_{\rm fs}$ from First Galaxies

The "warmth" of dark matter has (at least) two consequences: i) the power spectrum cut-off factor $\tau^2(k)$ described in Sections 3 and 4; and ii) the velocity dispersion cut-off mass $M_{\rm vd}$ of first galaxies, summarized in Table 2 [8]. Density perturbations with linear mass $M_{\rm vd}$ (as defined by the Press-Schechter formalism [7]) form galaxies with a delay $\Delta z = 1$ with respect to the cold dark matter case, and, somewhat below the mass $M_{\rm vd}$, galaxies do not form at all. Comparing the mass of first galaxies $\approx 10^{8.7}$ M$_\odot$ in Fig. 11 of [10] with Table 2 we conclude that 1.6 Mpc$^{-1} \lesssim k_{\rm fs} \lesssim 3$ Mpc^{-1}. The corresponding range of $v_{h\rm rms}(1)$ is 470 to 250 m/s. The stellar mass, or ultraviolet luminosity, distributions of galaxies also obtain estimates of $M_{\rm vd}$, see for example [7].

6 Estimates of $k_{\rm fs}$ from Reionization

The hydrogen in the universe is neutral from about $z \approx 1000$ to $z \approx 10$. First stars ionize the hydrogen. The bulk of reionization occurs in the redshift range 8 to 6. The free electrons result in a reionization optical depth $\tau = 0.054 \pm 0.007$ measured by the Planck collaboration [1]. This measured reionization optical depth requires a cut-off in the galaxy luminosity distribution. From Table 3, and the discussion in [8], we estimate $v_{h\rm rms}(1)$ between 150 m/s and 1200 m/s.

7 A Journey to the Past

We have measured $v_{h\rm rms}(1) = 406 \pm 69$ m/s, see Table 1. Let us assume that dark matter is a gas of particles of mass m_h. We can define the temperature of dark matter in terms of its mean energy per particle. For particles in a box

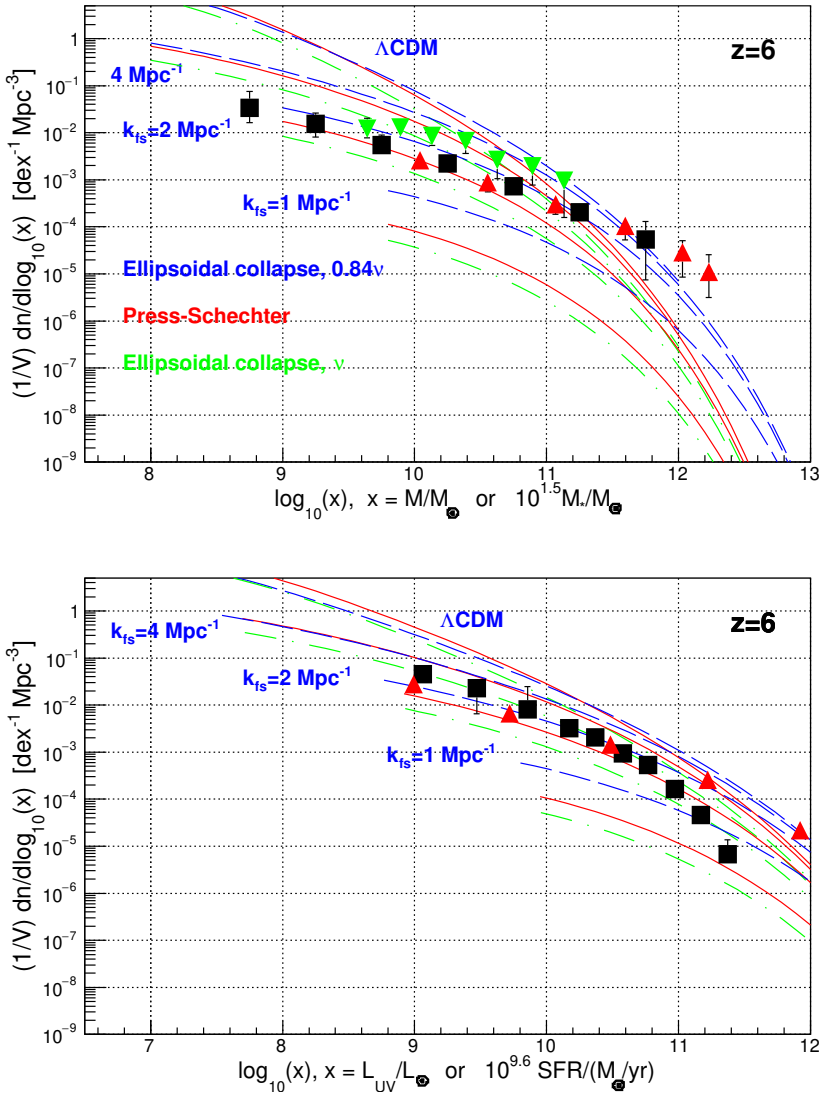

Figure 7: Comparison of predicted and observed distributions of $M/M_\odot = 10^{1.5} M_*/M_\odot$ (top panel) and $L_{UV}/L_\odot = 10^{9.6}\mathrm{SFR}/(M_\odot/\mathrm{yr})$ (bottom panel) for redshift $z = 6$. M is the linear total mass of the perturbation (as defined by the Press-Schechter formalism). M_* is the stellar mass of the galaxy. Data are from the Hubble Space Telescope (M_* from [17] and L_{UV} from [18]) (black squares), from the continuity equation [19] (red triangles), and from the James Webb Space Telescope (green triangles) [20]. Three predictions are shown for each k_{fs} to illustrate the uncertainty of the predictions. Figure from [7].

Table 2: Shown is the velocity dispersion cut-off mass $M_{\rm vd}$ of the linear total (dark matter plus baryon) mass M (as defined by the Press-Schechter formalism), as a function of redshift z and of the free-streaming comoving cut-off wavenumber $k_{\rm fs}(t_{\rm eq})$. At this cut-off mass $M_{\rm vd}$, velocity dispersion delays galaxy formation by $\Delta z = 1$ (obtained from numerical integration of hydro-dynamical equations). Table from [8].

z	$k_{\rm fs}(t_{\rm eq})$ [Mpc^{-1}]	$M_{\rm vd}$ [$M_\odot$]	z	$k_{\rm fs}(t_{\rm eq})$ [Mpc^{-1}]	$M_{\rm vd}$ [$M_\odot$]
4	1	1.5×10^9	8	1	2×10^{10}
4	1.66	3×10^8	8	1.66	4×10^9
4	2	2×10^8	8	2	1.5×10^9
4	4	3×10^7	8	4	1.5×10^8
6	1	6×10^9	10	1	2×10^{10}
6	1.66	2×10^9	10	1.66	4.5×10^9
6	2	1×10^9	10	2	2×10^9
6	4	1×10^8	10	4	2×10^8

Table 3: At $z = 8$, for each $k_{\rm fs}(t_{\rm eq})$ are presented the velocity dispersion cut-off $M_{\rm vd}/M_\odot$ of the linear total (dark matter plus baryon) mass $M/M_\odot \approx L_{\rm UV}/L_\odot$, the corresponding cut-off AB-magnitude $M_{\rm UV} \approx 5.9 - 2.5 \log_{10}(L_{\rm UV}/L_\odot)$, and the reionization optical depth τ from Fig. 13 of [21]. A somewhat lower value of τ is obtained from Fig. 2 of [22]. The Planck collaboration obtains $\tau = 0.054 \pm 0.007$ [1]. Table from [8].

$k_{\rm fs}(t_{\rm eq})$	$M_{\rm vd}/M_\odot$	$M_{\rm UV}$ cut-off	τ
1 Mpc^{-1}	2×10^{10}	-19.9	0.047 ± 0.006
2 Mpc^{-1}	1.5×10^9	-17.0	0.053 ± 0.006
4 Mpc^{-1}	1.5×10^8	-14.5	0.060 ± 0.008

of side a, the momenta are proportional to a^{-1}, so an ultra-relativistic gas has a temperature $T(a) \propto a^{-1}$, while for a non-relativistic gas $T(a) \propto a^{-2}$. For dark matter, these two asymptotes meet at the expansion parameter

$$a_{h\mathrm{NR}} \approx \frac{v_{h\mathrm{rms}}(1)}{c} = (1.35 \pm 0.23) \times 10^{-6}. \tag{14}$$

The comoving temperature of the non-relativistic gas can be defined as

$$\frac{1}{2} m_h v_{h\mathrm{rms}}^2(1) \equiv \frac{3}{2} k T_h(1). \tag{15}$$

So, the measurements of $v_{h\mathrm{rms}}^2(1)$ are measurements of the dark matter temperature-to-mass ratio. We would like to obtain separately the dark matter temperature and mass. The present number density of dark matter particles is

$$n_h(1) = \frac{\Omega_c \rho_{\mathrm{crit}}}{m_h}. \tag{16}$$

Due to the expansion of the universe, decoupled and conserved dark matter, whether ultra-relativistic or non-relativistic, has a number density

$$n_h(a) = n_h(1) a^{-3}. \tag{17}$$

This equation assumes dark matter particles do not decay or annihilate when they become non-relativistic at $a \approx a_{h\mathrm{NR}}$, i.e. if there is no "freeze-out". At $a = a_{h\mathrm{NR}}$,

$$n_h(a_{h\mathrm{NR}}) \approx \frac{\Omega_c \rho_{\mathrm{crit}}}{m_h} \left(\frac{c}{v_{h\mathrm{rms}}(1)} \right)^3, \tag{18}$$

$$T_h(a_{h\mathrm{NR}}) \approx \frac{m_h c^2}{3k}. \tag{19}$$

The photon temperature at $a_{h\mathrm{NR}}$ is

$$T_\gamma(a_{h\mathrm{NR}}) \approx T_0 \frac{c}{v_{h\mathrm{rms}}(1)}, \tag{20}$$

so

$$\frac{T_h(a_{h\mathrm{NR}})}{T_\gamma(a_{h\mathrm{NR}})} \approx \frac{m_h c v_{h\mathrm{rms}}(1)}{3 k T_0}. \tag{21}$$

This is as far as we can go without further assumptions.

8 Zero chemical potential

Let us now assume that the ultra-relativistic dark matter gas has zero chemical potential in the very early universe (an assumption that needs confirmation). Zero chemical potential of dark matter is equivalent to the assumption that in the early universe dark matter is in thermal and diffusive contact, i.e. can exchange energy and particles, and is in equilibrium, with "something", and the total number of dark matter particles is not conserved, i.e. has no conserved quantum number. Then the chemical potential will remain zero while ultra-relativistic, even after decoupling. This assumption breaks the degeneracy between dark matter mass and temperature. An ultra-relativistic gas with zero chemical potential has a number density

$$n(T) = \frac{\zeta(3)}{\pi^2} \cdot \left(\frac{kT}{\hbar c}\right)^3 \left(N_b + \frac{3}{4}N_f\right), \tag{22}$$

where $\zeta(3)/\pi^2 \approx 0.1218$. N_b and N_f are the numbers of boson and fermion distinct states. From (18), (19), (21) and (22) we obtain approximately

$$m_h \approx \left(\frac{\Omega_c \rho_{\rm crit} (3\hbar)^3}{0.1218 \cdot v_{h\rm rms}^3(1)}\right)^{1/4} (N_b + 3N_f/4)^{-1/4}, \tag{23}$$

or

$$m_h \approx 107.2 \text{ eV} \left(\frac{760 \text{ m/s}}{v_{h\rm rms}(1)}\right)^{3/4} (N_b + 3N_f/4)^{-1/4}, \tag{24}$$

and

$$\frac{T_h(a_{h\rm NR})}{T_\gamma(a_{h\rm NR})} \approx 0.386 \left(\frac{v_{h\rm rms}(1)}{760 \text{ m/s}}\right)^{1/4} (N_b + 3N_f/4)^{-1/4}. \tag{25}$$

(There is a disagreement between (24) and limits on m_h from the Lyman-α forest of quasar light that will be addressed in Section 10 below.)

A more exact (but model-dependent) prediction is obtained in [23]. Ultra-relativistic dark matter is assumed to have zero chemical potential, and the ultra-relativistic Bose-Einstein or Fermi-Dirac energy-momentum distribution. Then it is assumed that non-relativistic dark matter relaxes to the corresponding non-relativistic Bose-Einstein or Fermi-Dirac momentum distribution, thereby acquiring a negative chemical potential when non-relativistic.

From Equations (28) of [23] for **bosons** we obtain

$$m_h = 108.5 \text{ eV } \left(\frac{760 \text{ m/s}}{v_{h\text{rms}}(1)}\right)^{3/4} N_b^{-1/4}, \tag{26}$$

$$T_h(1) = 2.86 \times 10^{-6} K N_b^{-1/4} \left(\frac{v_{h\text{rms}}(1)}{760 \text{ m/s}}\right)^{5/4}, \tag{27}$$

$$a_{h\text{NR}} \approx \sqrt{\frac{3kT_h(1)}{m_h c^2}} = 1.03 \left(\frac{v_{h\text{rms}}(1)}{c}\right), \tag{28}$$

$$\frac{T_h(a_{h\text{NR}})}{T_\gamma(a_{h\text{NR}})} \approx 0.402 \left(\frac{v_{h\text{rms}}(1)}{760 \text{ m/s}}\right)^{1/4} N_b^{-1/4}. \tag{29}$$

From Equations (26) of [23] for **fermions** we obtain

$$m_h = 128.9 \text{ eV } \left(\frac{760 \text{ m/s}}{v_{h\text{rms}}(1)}\right)^{3/4} N_f^{-1/4}, \tag{30}$$

$$T_h(1) = 3.10 \times 10^{-6} K N_f^{-1/4} \left(\frac{v_{h\text{rms}}(1)}{760 \text{ m/s}}\right)^{5/4}, \tag{31}$$

$$a_{h\text{NR}} \approx \sqrt{\frac{3kT_h(1)}{m_h c^2}} = 0.98 \left(\frac{v_{h\text{rms}}(1)}{c}\right), \tag{32}$$

$$\frac{T_h(a_{h\text{NR}})}{T_\gamma(a_{h\text{NR}})} \approx 0.456 \left(\frac{v_{h\text{rms}}(1)}{760 \text{ m/s}}\right)^{1/4} N_f^{-1/4}. \tag{33}$$

In summary, if conserved ultra-relativistic dark matter has zero chemical potential, then the measured $v_{h\text{rms}}(1)$ determines both the mass m_h of dark matter particles, and the ratio $T_h(a_{h\text{NR}})/T_\gamma(a_{h\text{NR}})$, i.e. the ratio of dark matter-to-photon temperature after e^+e^- annihilation while dark matter is still ultra-relativistic. The measured $v_{h\text{rms}}(1)$ obtains $T_h(a_{h\text{NR}})/T_\gamma(a_{h\text{NR}})$ of order 1, which is a miracle given that m_h is unknown over 89 orders of magnitude, and the ratio also depends on T_0 and $\Omega_c\rho_{\text{crit}}$ (see (21) and (23)), and is surely telling us something! That $T_h(a_{h\text{NR}})/T_\gamma(a_{h\text{NR}})$ is less than 1 makes it possible that dark matter and the Standard Model sector are in thermal and diffusive equilibrium in the early universe. Let me explain. As the universe expands and cools, Standard Model particles become non-relativistic and annihilate or decay, heating photons but not dark matter (if dark matter has already decoupled from the Standard Model sector). Furthermore, $T_h(a_{h\text{NR}})/T_\gamma(a_{h\text{NR}})$ is sufficiently less than 1 to evade problems with big-bang nuleosynthesis (if decoupling is sufficiently early [11]).

9 No Freeze-In and no Freeze-Out

Let us consider the following scenario. Dark matter is in thermal and diffusive equilibrium with the early Standard Model sector, i.e. no "freeze-in", decouples from the Standard Model sector while still ultra-relativistic, and does not decay or annihilate when dark matter becomes non-relativistic, i.e. no "freeze-out". To understand this scenario, it is convenient to study Fig. 8. Diffusive equilibrium with the Standard Model sector implies that dark matter has zero chemical potential while ultra-relativistic. Let us recall that an ultra-relativistic gas, in thermal equilibrium and with zero chemical potential, has the following entropy density:

$$s(T) \;=\; \frac{2\pi^2}{45}\cdot\left(\frac{kT}{\hbar c}\right)^3\left(N_b+\frac{7}{8}N_f\right), \tag{34}$$

From entropy conservation, the ratio of dark matter-to-photon temperature, after e^+e^- annihilation and before dark matter becomes non-relativistic, is

$$\frac{T_h}{T_\gamma}=\left(\frac{43}{11g_{\rm dec}}\right)^{1/3}, \tag{35}$$

where $g_{\rm dec}\equiv\sum N_b+(7/8)\sum N_f$ at decoupling of dark matter from the Standard Model sector [1].

As an example, consider dark matter with a contact coupling and in thermal and diffusive equilibrium with the Higgs boson. This dark matter becomes decoupled from the Standard Model sector when the Higgs boson becomes non-relativistic and decays. In this case $g_{\rm dec}=95.25$ and

$$\frac{T_h}{T_\gamma}=0.345, \tag{36}$$

see Fig. 8. If instead, the coupling is to the top quark, $g_{\rm dec}=96.25$ and $T_h/T_\gamma=0.344$. At the other extreme, if the coupling is to the strange quark, $g_{\rm dec}=51.25$ and $T_h/T_\gamma=0.424$. Decoupling at lower temperature compromises big-bang nucleosynthesis [11].

From (35) and $N_b=2$ for photons, the ratio of number densities of dark matter particles and photons, after e^+e^- annihilation until the present time, assuming dark matter has zero chemical potential while ultra-relativistic, is

$$\frac{n_h}{n_\gamma}=\frac{43g_h'}{22g_{\rm dec}}, \tag{37}$$

where $g_h'=N_b+3N_f/4$ for the dark matter. Then, at the present time,

$$n_h(1)=\frac{\Omega_c\rho_{\rm crit}}{m_h}=\frac{43g_h'}{22g_{\rm dec}}0.1218\left(\frac{kT_0}{\hbar c}\right)^3\cdot 2, \tag{38}$$

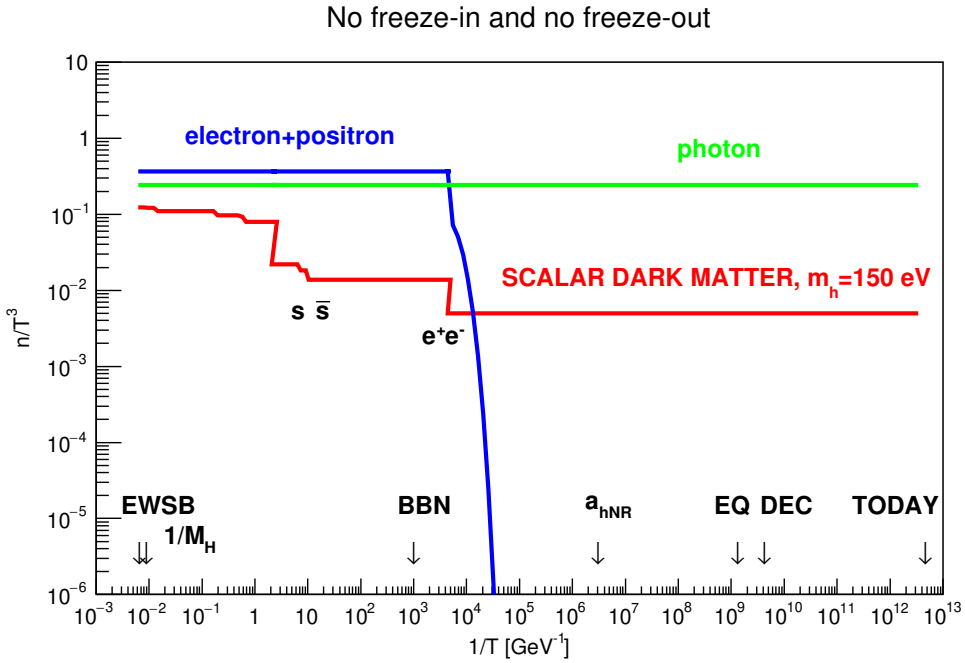

Figure 8: The "no freeze-in and no freeze-out" dark matter scenario is illustrated for spin zero warm dark matter particles coupled to the Higgs boson. T is the *photon* temperature, and the n's are particle number densities. The abbreviations stand for "Electro-Weak Symmetry Breaking", "Big Bang Nucleosynthesis", "EQuivalence" of matter and radiation densities, and "DECoupling" of photons from the proton-electron plasma when it recombines to neutral hydrogen. Dark matter particles become non-relativistic at $a_{h\mathrm{NR}}$. Time advances towards the right. Figure from [3].

or

$$\Omega_c h^2 = \frac{n_h(1) m_h h^2}{\rho_{\mathrm{crit}}} \approx 76.2 \frac{g'_h}{g_{\mathrm{dec}}} \frac{m_h}{\mathrm{keV}}, \tag{39}$$

determines the dark matter particle mass m_h corresponding to no freeze-in and no freeze-out. From (21) and (35) we obtain

$$v_{h\mathrm{rms}}(1) \approx \left(\frac{43}{11 g_{\mathrm{dec}}}\right)^{1/3} \frac{3kT_0}{m_h c}. \tag{40}$$

This equation and the measured $v_{h\mathrm{rms}}(1)$, together with (26) or (30), obtain the decoupling g_{dec}.

The predictions and measurements are compared in Table 4 for the case when dark matter is coupled to the Higgs boson. The measurements are

Table 4: Comparison of predictions and measurements, for several dark matter spins, assuming dark matter is coupled to the Higgs boson, and the measured $v_{h\mathrm{rms}}(1) = 406 \pm 69$ m/s. T_h/T_γ is the ratio of dark matter-to-photon temperatures after e^+e^- annihilation. Predictions are from (35), (39), and (26) or (30) with the predicted m_h. Similar predictions of $v_{h\mathrm{rms}}(1)$ are obtained from (40). Measurements are from (26) to (33) with the measured $v_{h\mathrm{rms}}(1)$. Predictions for spin 0 dark matter are consistent with measurements. For non-zero spins the predicted $v_{h\mathrm{rms}}(1)$ is larger than the measurement.

DM spin	g'_h	Prediction T_h/T_γ	Prediction m_h	Prediction $v_{h\mathrm{rms}}(1)$	Measurement T_h/T_γ	Measurement m_h
0	1	0.345	150 eV	493 m/s	0.343 ± 0.015	177 ± 23 eV
1	3	0.345	50 eV	1480 m/s	0.260 ± 0.011	135 ± 17 eV
1/2 Majorana	3/2	0.345	100 eV	846 m/s	0.327 ± 0.014	177 ± 23 eV
1/2 Dirac	3	0.345	50 eV	1692 m/s	0.275 ± 0.012	149 ± 19 eV

consistent with spin zero dark matter. For higher dark matter spin the predicted $v_{h\mathrm{rms}}(1)$ are higher than the measurements.

10 Discrepancy with Lyman-α Forest Limits

Studies of the Lyman-α forest of quasar light set limits to the dark matter "thermal relic" mass, typically of order 550 eV [24] up to 5700 eV [25], that are in disagreement with each of the measurements in Table 1.

The Lyman-α forest limits are really limits on the power spectrum of density fluctuations cut-off factor $\tau^2(k)$ due to warm dark matter free-streaming. This cut-off factor for dark matter that was once in thermal equilibrium with the Standard Model sector, and decouples early-on from this sector, is obtained in [24] by solving Boltzmann code simulations (either CMBFAST or CAMB):

$$\tau^2(k) = \left[1 + (\alpha k)^{2\nu}\right]^{-10/\nu}, \tag{41}$$

$$\alpha = 0.049 \left(\frac{m_h}{1\ \mathrm{keV}}\right)^{-1.11} \left(\frac{\Omega_c}{0.25}\right)^{0.11} \left(\frac{h}{0.7}\right)^{1.22} h^{-1}\ \mathrm{Mpc}, \tag{42}$$

with $\nu = 1.12$. This $\tau^2(k)$ is used in many Lyman-α studies. For comparison

with (11), we can approximate (41) by $\tau^2(k) \approx \exp\left[-k^2/k_{\rm fs}^2\right]$ with

$$k_{\rm fs} \approx \frac{1}{2.6\alpha} \approx \left(\frac{m_h}{1\ {\rm keV}}\right)^{1.11} 5.6\ {\rm Mpc}^{-1}. \tag{43}$$

For comparison, $k_{\rm fs}(t_{\rm eq})$ in (12) can be estimated as a function of the dark matter particle mass m_h using (40). The result (for coupling to the Higgs boson to be specific) is

$$k_{\rm fs}(t_{\rm eq}) \approx \left(\frac{m_h}{1\ {\rm keV}}\right) 10.3\ {\rm Mpc}^{-1}. \tag{44}$$

(A similar alternative value of $k_{\rm fs}(t_{\rm eq})$ is obtained from (26) or (30), which obtain $k_{\rm fs}(t_{\rm eq}) \propto m_h^{1.33}$.)

We note that $k_{\rm fs}$ in (43) differs from $k_{\rm fs}(t_{\rm eq})$ in (44) by a factor ≈ 2 for a given m_h. However, our main difference is the measured non-linear regenerated "tail" in (13), that is lacking in (41).

Let us mention that the Lyman-α forest of quasar light is sensitive to neutral hydrogen density fluctuations. However, most of the hydrogen is in an ionized state [26] due to re-ionization by active galactic nuclei and stellar ultra-violet light. The correlation between neutral hydrogen density fluctuations and $\tau^2(k)$ is non-trivial.

The measured $v_{h{\rm rms}}(1) = 406 \pm 69$ m/s in Table 1 implies $k_{\rm fs} = 1.9 \pm 0.3\ {\rm GeV}^{-1}$ from (12), as can be seen directly in Fig. 7. The tightest Lyman-α forest limit $m_h > 5700$ eV [25] implies $k_{\rm fs} > 39\ {\rm GeV}^{-1}$ from (43). So, indeed, there is a discrepancy between each of the measurements in Table 1 and the interpretation of the Lyman-α forest of quasar light. Either each measurement in Table 1 is wrong (even tho they use independent data sets and different observables, and the measurements from rotation curves are independent of $\tau^2(k)$), or the interpretation of the Lyman-α forest of quasar light is wrong. In any case, the measurements of $v_{h{\rm rms}}(1)$ presented in Figs. 1 and 2 are more direct than the limits from the Lyman-α forest, see [25]. If the Lyman-α limit holds, then (25) or (29) or (33) obtain a wrong ratio T_h/T_γ. The present article is published because both the interpretation of the Lyman-α forest and each of the measurements in Table 1 have their own delicate issues, and these discrepancies need to be understood.

11 Conclusions

From the studies summarized in this article, we obtain the following conclusions:

1. The dark matter temperature-to-mass ratio, or equivalently, the adiabatic invariant $v_{h\mathrm{rms}}(1) \equiv v_{h\mathrm{rms}}(a)a$ of cosmological origin, has been measured with multiple independent data sets, and several independent observables. The results are consistent, see Table 1.

2. Galaxies with warm dark matter have a dark matter core, not a cusp, see Figs. 1 and 5 (these cores are observed in dwarf galaxies, but are too small to be resolved in most elliptical galaxies). The cores may form nearly adiabatically.

3. For warm dark matter, first galaxies have a velocity dispersion cut-off mass presented in Table 2.

4. The most reliable measurement of $v_{h\mathrm{rms}}(1)$ is obtained from the rotation curves of these first dwarf galaxies, because the relaxation and dark matter halo rotation corrections are relatively small (compare Fig. 2 with Fig. 4). The result is

$$v_{h\mathrm{rms}}(1) = 406 \pm 69 \text{ m/s}. \tag{45}$$

5. Future more detailed studies of dwarf galaxies, with next generation instruments, should be able to reduce this uncertainty on $v_{h\mathrm{rms}}(1)$.

6. The measured $v_{h\mathrm{rms}}(1)$, together with the assumption that ultra-relativistic dark matter has zero chemical potential, happens to be in agreement with the "no freeze-in and no freeze-out" scenario of spin zero dark matter that reaches thermal and diffusive equilibrium with, and decouples early on from, the Standard Model sector, while still ultra-relativistic. This scenario is presented in Fig. 8 for dark matter with a contact coupling to the Higgs boson. Predictions and measurements are compared in Table 4. Note that predictions and measurements are in agreement if dark matter has spin zero. Majorana dark matter with spin 1/2 is disfavored by more than 5 standard deviations, and is (almost) ruled out for this specific scenario. For spin zero dark matter, with (45), (26) and (29), we *measure*

$$m_h = 177 \pm 23 \text{ eV}, \tag{46}$$

and a dark matter-to-photon temperature ratio after e^+e^- annihilation

$$\frac{T_h}{T_\gamma} = 0.343 \pm 0.015, \tag{47}$$

sufficiently cold to not upset big-bang nucleosynthesis. Note that these *measured* T_h/T_γ and m_h are in agreement with the no freeze-in and no freeze-out scenario predictions, see Table 4.

7. Limits on $\tau^2(k)$ from studies of the Lyman-α forest of quasar light are inconsistent with each of the measurements in Table 1. These discrepancies need to be understood. In any case, the measurements of $v_{h\mathrm{rms}}(1)$ presented in Figs. 1 and 2 are more direct than the limits from the Lyman-α forest, see [25], and, furthermore, do not depend on $\tau^2(k)$. If the Lyman-α limit holds, then (25) or (29) or (33) obtain a wrong ratio T_h/T_γ.

8. Let us assume Table 1 is correct. The null results of direct and indirect dark matter searches implie that the dark matter interaction with the Standard Model sector is probably not mediated by the $U(1)$, $SU(2)$ or $SU(3)$ gauge bosons. We therefore consider a contact interaction. The simplest alternative is, arguably, a contact coupling to the Higgs boson field ϕ of the form $-\frac{1}{2}\lambda_{hS}(\phi^\dagger\phi)S^2$ with $|\lambda_{hS}| \approx 10^{-6}$ [27], where S is a dark matter real scalar field with Z_2 symmetry, i.e. $S \leftrightarrow -S$. If S participates in inflation, a quadratic and a quartic self-interaction is needed [28], as well as a non-minimal coupling to the scalar Ricci curvature [29]. In an interesting extension of the Standard Model, the scalar S is complex, and decays to two vector dark matter particles, $S \to V_\mu V^\mu$ [27].

Acknowledgements

I thank Karsten Müller for his early interest in this work and for many useful discussions.

References

[1] R.L. Workman et al. (Particle Data Group) The Review of Particle Physics (2023), Prog. Theor. Exp. Phys, 083C01.

[2] Hoeneisen, B. (2023) Understanding the Formation of Galaxies with Warm Dark Matter. *Journal of Modern Physics*, **14**, 1741-1754. https://doi.org/10.4236/jmp.2023.1413103

[3] Hoeneisen, B. (2023) A Data Driven Solution to the Dark Matter Problem. *European Journal of Applied Sciences*, **11**. DOI:10.14738/aivp.112.14383.

[4] Hoeneisen, B. (2022) Measurement of the Dark Matter Velocity Dispersion with Dwarf Galaxy Rotation Curves. *Inter-*

national Journal of Astronomy and Astrophysics, **12**, 363-381. https://doi.org/10.4236/ijaa.2022.124021

[5] Hoeneisen, B. (2019) The Adiabatic Invariant of Dark Matter in Spiral Galaxies. *International Journal of Astronomy and Astrophysics*, **9**, 355-367. https://doi.org/10.4236/ijaa.2019.94025

[6] Hoeneisen, B. (2024) Understanding Elliptical Galaxies with Warm Dark Matter, in review.

[7] Hoeneisen, B. (2024) Are James Webb Space Telescope Observations Consistent with Warm Dark Matter? *International Journal of Astronomy and Astrophysics*, **14**, 45-60. https://doi.org/10.4236/ijaa.2024.141003

[8] Hoeneisen, B. (2022) Measurement of the Dark Matter Velocity Dispersion with Galaxy Stellar Masses, UV Luminosities, and Reionization. *International Journal of Astronomy and Astrophysics*, **12**, 258-272. https://doi.org/10.4236/ijaa.2022.123015

[9] Hoeneisen, B. (2022) Warm Dark Matter and the Formation of First Galaxies, *Journal of Modern Physics*, **13**, 932-948.

[10] Marr, J.H. (2020) The Dynamics of Globular Clusters and Elliptical Galaxies. arxiv:2008.01424

[11] Hoeneisen, B. (2019) A Study of Dark Matter with Spiral Galaxy Rotation Curves. *International Journal of Astronomy and Astrophysics*, **9**, 71-96. https://doi.org/10.4236/ijaa.2019.92007

[12] Oh, S. *et al.* (2015) High-Resolution Mass Models of Dwarf Galaxies from LITTLE THINGS, *Astronomical Journal* **149**, doi:10.1088/0004-6256/149/6/180

[13] Karukes, E.V., Salucci, P. (2017) The Universal Rotation Curve of Dwarf Disc Galaxies MNRAS **465**, 4703-4722

[14] Lelli F., McGaugh S. S., Schombert (2016), SPARC: Mass models for 175 disk galaxies with Spitzer Photometry and Accurate Rotation Curves *The Astronomical Journal* **152**. doi:10.3847/0004-6256/152/6/157

[15] Shajib, A.J., Treu, T., Birrer, S., Sonnenfeld, A. (2021) Dark Matter Halos of Massive Elliptical Galaxies at z = 0.2 are well Described by the Navarro-Frenk-White Profile. MNRAS **503**

[16] Boyanovsky, D., de Vega, H.J., Sanchez, N.G. (2008) The dark matter transfer function: free streaming, particle statistics and memory of gravitational clustering. *Physical Review D*, **78**, Article ID: 063546.

[17] Song. M., *et al.* (2016) The Evolution of the Galaxy Stellar Mass Function at $z = 4 - 8$: A Steepening Low-Mass-End Slope with Increasing Redshift. *The Astrophysical Journal* **825**

[18] Bouwens, R.J., *et al.* (2021) New Determinations of the Luminosity Functions from $z \approx 9$ to $z \approx 2$ show Remarkable Consistency with Halo Growth and a Constant Star Formation Efficiency, *The Astronomical Journal* **162**

[19] Lapi, A., Salucci, P., Danese, L. (2018) Precision Scaling Relations for Disk Galaxies in the Local Universe. *The Astrophysical Journal* **859**.

[20] Navarro-Carrera, R., Rinaldi, P., Caputi, K.I., Iani, E., Kokorev, V., van Mierlo, S. (2024) Constraints on the Faint End of the Galaxy Stellar Mass Function at $z \approx 4$ - 8 from Deep JWST Data.
The Astrophysical Journal, **961**

[21] Mason, C.A., Trenti, M., Treu, T. (2015) The Galaxy UV Luminosity Function Before the Epoch of Reionization. *The Astrophysical Journal* **813**

[22] Lapi, A., Danese, L. (2015) Cold or Warm? Constraining Dark Matter with Primeval Galaxies and Cosmic Reionization after Planck. *Journal of Cosmology and Astroparticle Physics* **9**

[23] Paduroiu, S., Revaz, Y., Pfenniger, D. (2015) Structure formation in warm dark matter cosmologies Top-Bottom Upside-Down arxiv:1506.03789

[24] Viel M., Lesgourgues J., Haehnelt M. G., Matarrese S., Riotto A. (2005), Constraining Warm Dark Matter candidates including sterile neutrinos and light gravitinos with WMAP and the Lyman- forest, *Phys. Rev. D*, **71**, 063534

[25] Iršič, V. and Viel. M. and Martin G. (2024) Unveiling Dark Matter free-streaming at the smallest scales with high redshift Lyman-alpha forest arxiv:2309.04533

[26] Georgiev, I., Mellema, G., and Giri, S.K. (2024) The forest at EndEoR: The effect of Lyman Limit Systems on the End of Reionisation, arxiv:2405.12273

[27] Hoeneisen, B. (2021) Adding Dark Matter to the Standard Model. *International Journal of Astronomy and Astrophysics*, **11**, 59-72. https://doi.org/10.4236/ijaa.2021.111004

[28] Hoeneisen, B. (2023) Exploring Inflation Options for Warm Dark Matter Coupled to the Higgs Boson. *International Journal of Astronomy and Astrophysics*, **13**, 217-235. https://doi.org/10.4236/ijaa.2023.133013

[29] Bezrukov, F., Shaposhnikov, M. (2008) The Standard Model Higgs boson as the inflaton, *Phys.Lett.B* **659**